Design and Analytical Performances of a Diclofenac Biosensor for Water Resources Monitoring

Yacine Mazouzi, Antoine Miche, Alexis Loiseau, Bruno Beito, Christophe Méthivier, Dietmar Knopp, Michèle Salmain, Souhir Boujday

Design and analytical performances of a diclofenac biosensor for water resources monitoring

Yacine Mazouzi[1], Antoine Miche[1], Alexis Loiseau[1], Bruno Beito[1], Christophe Méthivier[1], Dietmar Knopp[3], Michèle Salmain[2,*], Souhir Boujday[1,*]

[1] Sorbonne Université, CNRS, Laboratoire de Réactivité de Surface (LRS), 4 place Jussieu, F-75005 Paris, France.

[2] Sorbonne Université, CNRS, Institut Parisien de Chimie Moléculaire (IPCM), 4 place Jussieu F-75005 Paris, France.

[3] Technical University Munich, Chair of Analytical Chemistry and Water Chemistry, Institute of Hydrochemistry, Marchioninistrasse 17, 81377 München, Germany

KEYWORDS: Immunosensor, Non-steroidal anti-inflammatory drug, Antibody, Quartz Crystal Microbalance, Nanoplasmonics

ABSTRACT: Because the broadly consumed pain killer diclofenac (DCF) is a recognized pollutant, monitoring of its concentration is routinely performed in surface waters. As a valuable alternative to chromatographic and immunochemical assays, we developed a piezoelectric immunosensor to quantify DCF, first in buffer (PBS) and then in river water samples. A sensing layer comprising DCF was built up on the surface of silica-coated quartz sensors using a robust coupling chemistry. Binding of a highly affine monoclonal anti-DCF antibody was monitored in real time by quartz crystal microbalance with dissipation (QCM-D) measurements from which were determined a dissociation constant K_D of 0.24 nM and an acoustic antibody surface coverage of 1120 ng/cm² at saturation. On the other hand, an optical antibody surface coverage of 260 ng/cm² was determined by combined nanoplasmonic sensing measurement, giving a hydration percentage of 75% for the antibody monolayer. DCF assay was further set up following an competitive format for which binding of antibody to the sensing layer is inhibited by DCF in solution. The piezoelectric sensor response expressed as frequency shift ΔF was inversely related to the concentration of DCF with a dynamic range of 15 – 46 nM and a limit of detection (LoD) of 9.5 nM (2.8 µg/L) in PBS. This piezoelectric immunosensor was eventually applied to the assay of DCF in surface water samples taken at three different locations in the Seine and the Marne rivers. The calculated concentration of DCF in these samples was in good agreement with official data published by the French center of water analysis eaufrance.

Diclofenac (DCF), a non-steroidal anti-inflammatory drug (NSAID), is one of the most consumed pain killers worldwide with, for instance, 80 to 100 tons/year consumed in Germany and 40 to 60

ton/year in France.[1] As a result, and because of inefficient waste water treatment processes, DCF is considered as an emerging water pollutant and was listed in the first watch list of ten organic molecules to be monitored and reported.[2,3] DCF is suspected to be hazardous to the aquatic environment[4] and in turn to human health. In 2019, the French agency for food safety and environment (ANSES) published a notice on the possible sanitary consequences of the presence of DCF in surface water and edited a guide value of 0.4 µg/L.[5]

Chromatographic methods are routinely used to quantify DCF residues in surface and ground water.[6,7] Alternatively, label-based immunochemical assays allow to quantify DCF in water samples with sensitivities from the µg/L down to the sub ng/L range, depending on the detection method.[8–17] Although these methods are selective and sensitive, they are not easily amenable to on-site detection. In this context, various biosensing set ups have been implemented using antibodies,[18] aptamers[19,20] or even whole cells[21–23] as bioreceptors coupled to electrochemical[24–26] or optical[27,28] signal transduction. With such set ups, DCF could be quantified in various matrices with variable sensitivities.

DCF being a small molecule, the only possible assay format is of the competitive type, thus requiring to build up a sensing platform at the surface of the transducer comprising an analogue of the analyte that will compete with the analyte in solution to bind the antibody. Previously, we had introduced a reliable strategy to generate a sensing layer comprising DCF molecules at the surface of planar and nanostructured gold and silica substrates and its ability to bind a polyclonal anti-DCF antibody.[29,30] This led to the implementation of an automated, flow-through, enzyme-based competitive immunoassay of DCF using chemiluminescence readout with good analytical performances and shelf-life.[29]

In this work, we rely on this strategy to develop a label-free and fully regenerable piezoelectric immunosensor for the quantification of DCF in water samples. The sensing layer was carefully constructed at the surface of silica-coated QCM-D sensors with a slight modification regarding DCF immobilization thanks to an optimized activation process. Binding of a monoclonal highly affine anti-DCF antibody (mAb) developed by some of us[15] to silica-coated quartz sensors functionalized by DCF was monitored in real time by quartz crystal microbalance with dissipation (QCM-D) measurement and by an original simultaneous combination of QCM-D and Localized Surface Plasmon Resonance (LSPR). This allowed to estimate the coverage and the hydration level of the formed monolayer; mAb appeared to form a highly hydrated monolayer. The competitive QCM-D immunosensing device to which we aspired in our previous studies, was built and tested in buffer media. For this sensor, the response is expressed as frequency shift, $\triangle F$, inversely related to the concentration of DCF in solution. We determined the analytical performances of our QCM-D immunosensor in terms of dynamic range (DR), limit of detection (LoD) and limit of quantification (LoQ). Eventually, this biosensor was employed to quantify DCF in river water samples collected at different spots in the Seine and Marne rivers in France.

EXPERIMENTAL SECTION

Materials, surface functionalization protocols and characterization techniques are presented in Supporting Information.

Anti-diclofenac antibody binding test and regeneration. Functionalized sensors were mounted in the QCM-D chambers and the following measurement cycle was applied. After signal stabilization in running buffer (0), mAb solution (1) was flown over the sensor substrate for approximatively 120 min. Then, the

sensor was rinsed with running buffer to remove unbound antibody. For reuse purpose, the regeneration buffer (2) was injected for 15 min prior to re-equilibration in running buffer for another 15 min. Antibody concentration optimization was conducted by injecting increasing solutions ranging from 0.05 to 5 mg/L at a flow rate of 50 µL/min. Flow rate impact on antibody binding was investigated by injecting anti-DCF antibody (1 mg/L) at 25 and 50 µL/min.

Combined QCM-D and LSPR measurements. For combined QCM-D and Localized Surface Plasmon Resonance (LSPR) measurements, the same experimental protocol was followed, except that mAb solution (5 mg/L) was injected for approximatively 110 min and the flow rate was set to 25 µL/min.

Competitive assay for diclofenac detection in buffer. For diclofenac immunosensing, the competitive format was employed with DCF covalently immobilized onto the sensor surface *via* the PyBOP procedure. Samples containing known concentrations of DCF ranging from 0 to 333.2 nM were pre-incubated with mAb (5 mg/L) during 60 min at 37 °C in either PBS or PBS/EtOH 9:1. The preincubated samples were flown over the substrate surface for 60 min at a flow rate of 25 µL/min and rinsed with running buffer for 15 min.

Quantification of diclofenac in surface water samples. Surface water samples (500 mL) were filtered through a 0.22 µm cellulose ester membrane filter (Millipore) to remove suspended matter and were kept in the dark at 4 °C until solid phase extraction (SPE). DCF were extracted following a modified procedure using Oasis HLB 3cc cartridge (Waters) without pH adjustment.[15] The cartridge was preconditioned with 1 mL of methanol followed by 1 mL of ultrapure water. The surface water sample was loaded onto the cartridge followed by washing with 1 mL of water/MeOH 95/5 (v/v). The cartridge was dried for 10 min under vacuum, and DCF was eluted with 1 mL of methanol and kept in the dark at 4 °C. Prior to QCM-D measurement, the extracts were dried under vacuum and the residues reconstituted with 5 mL of PBS. A 100-fold concentration factor was therefore obtained, assuming total recovery during SPE procedure. The water samples were preincubated with mAb (5 mg/L) during 60 min at 37 °C and then were flown over the substrate surface for 60 min at a flow rate of 25 µL/min and rinsed with running buffer for 15 min. Considering sample preconcentration, antibody incubation and frequency readout, the total assay time is close to 3 h. The frequency readout step can be reduced to 10 min, thus lowering the total assay time to ca. 2h.

RESULTS AND DISCUSSION

Surface functionalization. A sensing layer comprising a PEG layer bearing terminal amine functions, was built up on planar and nanostructured silica-coated quartz sensors as schematized in Figure 1, following a previously reported surface functionalization protocol.[29]

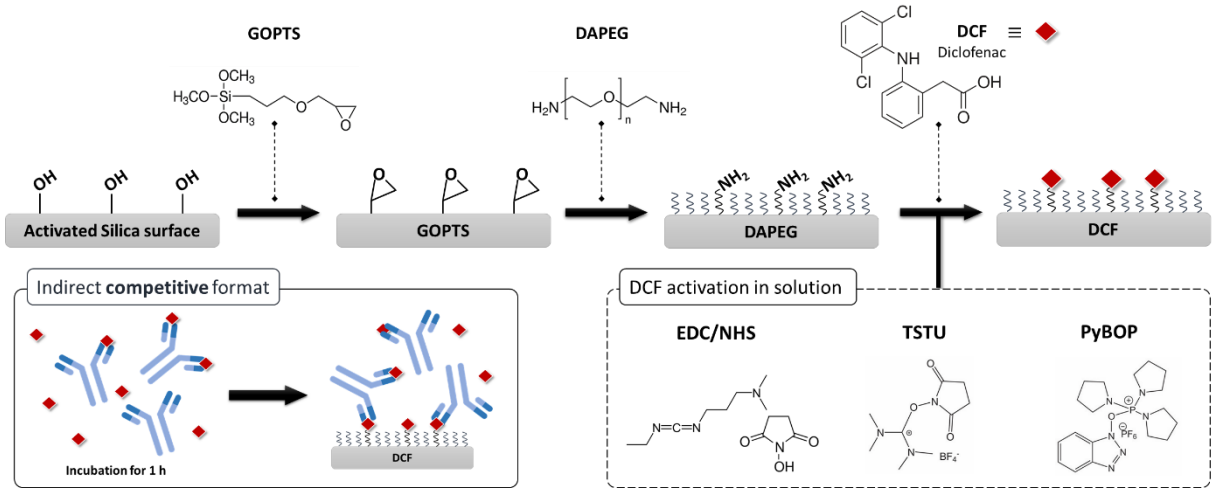

Figure 1. Formation of diclofenac sensing layer by step-by-step functionalization of silica / silicon surfaces and schematic representation of competitive assay format.

Experimental details and surface characterizations by ATR-IR, WCA and XPS are given in the supplementary information. Conjugation of DCF to the primary amine group of DAPEG requires preliminary activation of its carboxylic acid function. This was performed with three activation reagents, namely EDC/NHS, TSTU or PyBOP (Figure S3) with the objective of comparing the coupling efficiency and optimizing the number of analytes on the surface and, therefore, the sensing efficiency.

The presence of DCF at the surface of the sensors was investigated by XPS, taking advantage of the two chlorine atoms of DCF, possibly resulting in a chlorine Cl_{2p} photopeak at 200 eV. The resulting spectra and the corresponding atomic compositions are shown in Figure 2 and Table S2, respectively.

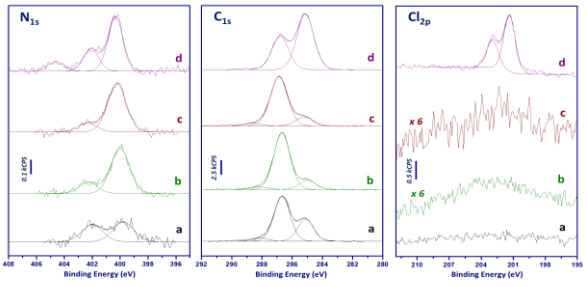

Figure 2. N_{1s}, C_{1s} and Cl_{2p} XPS spectra of Si substrates sequentially treated by (a) GOPTS and DAPEG; then by DCF activated *via* (b) EDC/NHS, (c) TSTU and (d) PyBOP.

For the three methods N_{1s} showed a change in contribution balance previously assigned to amide bonds formation.[29] Cl_{2p} and C_{1s} photopeaks showed differences between the activation reagents. First, the Cl_{2p} photopeak was barely detectable for EDC/NHS and TSTU but not for the PyBOP activation strategy, possibly due to a DCF surface concentration under the limit of detection of XPS in the two first cases. Second, the C_{1s} photopeak for PyBOP strategy was strongly modified: PEG contribution at 286.9 eV was attenuated while the aliphatic contribution at 285.2 eV increased in agreement with DCF grafting. The PyBOP strategy was further explored by analyzing the XPS peak intensities (Figure S4). The surface density in DCF was estimated to 2.3 molecules/nm² (detailed calculation is presented in Supporting Information). This value is slightly high and may result from excess physisorbed DAPEG and DCF. Indeed we followed by XPS analysis the removal of DCF when adding a sonication step and observed significant decrease of the Cl_{2p} signal (Figure S5). We further investigated the efficiency of the three activation reagents by comparing, by QCM-D, the binding of mAb to DCF-coated quartz sensors (Figure S6). We observed that regardless of the chosen activation reagent, mAb binding led to similar frequency shifts. This result and the observation of Chlorine XPS signal led us to select PyBOP for the following studies.

Biosensor design and regeneration.

First, the ability of the DCF-coated quartz sensor *via* PyBOP strategy to bind a monoclonal anti-DCF antibody (mAb) was investigated by QCM-D in flow-through mode (Figure 3A). Prior to antibody injection, stabilization was performed by flowing degassed PBS/EtOH 9:1. Then, mAb solution (5 mg/L) was injected at 50 µL/min for ca. 120 min after which the running buffer was flown again. Within this time frame, signal saturation was reached and the frequency and dissipation energy values shifted by -77 Hz and ~1 x 10^{-6}, respectively. The frequency shift was much higher in comparison to previous experiments conducted with a polyclonal anti-DCF antiserum for which a △F of -12 Hz shift was observed.[29] After flowing regeneration and rinsing buffers, the frequency and dissipation returned to their initial values. This shows the complete removal of bound antibody from the DCF sensing layer and a successful surface regeneration process.

One way to represent QCM-D data is by plotting the dissipation versus frequency, also referred as D-F plot (Figure 3B). This representation removes time as an explicit parameter and reveals $\Delta D - \Delta F$ relationship since it shows how much dissipation is induced by a frequency change.

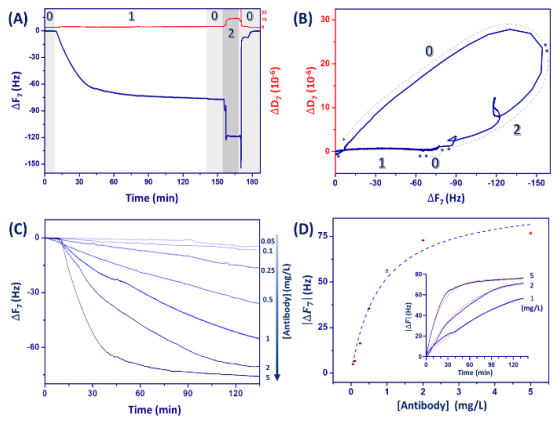

Figure 3. (A) QCM-D frequency and dissipation shifts upon injection of mAb solution (5 mg/L) to DCF modified quartz sensor at 50 µL/min and (B) the corresponding D-F plot. (0) running buffer, (1) mAb adsorption, (2) regeneration. (C) QCM-D frequency and dissipation shifts upon injection of mAb solution (0.05 - 5 mg/L) at 50 µL/min and (D) the corresponding saturation curve. QCM data used for the fit were added as an inset.

Antibody binding (step 1 in Figure 3B) was characterized by a linear relationship between dissipation and frequency shifts with a small slope of ~30 x 10^{-9} Hz^{-1} indicative of the formation of a rigid antibody layer.[31] Upon flowing buffer and regeneration solutions, large variations in both dissipation and frequency shifts can be observed. Through this data representation, full regeneration is illustrated by a loop going back to its starting point.

This experiment was repeated with mAb solutions ranging from 0.05 to 5 mg/L in running buffer as shown in Figure 3C. These solutions were flowed at 50 µL/min for ~120 min, followed by a washing step for 15 min. The absolute value of frequency shits were plotted as a function of mAb concentration (Figure 3D).

We have chosen to work at constant time rather than waiting for equilibrium which was reached at different times, depending on antibody concentrations. This allows us to be more rigorous in the evaluation of the analytical performances. The determination of the kinetic parameters, *i.e.* association (k_{on}) and dissociation (k_{off}) rate constants and the dissociation constant (K_D), was performed by curve fitting according to equation (2) during the antibody association phase (inset in Figure 3D).[32]

$$(2) \quad \Delta F(t) = \frac{\Delta F_{max} \times [Antibody]}{K_D + [Antibody]} \times \left(1 - \frac{1}{e^{(k_{on} \times [Antibody] + k_{off})t}}\right)$$

The detailed fit parameters are summarized in Table S3. From the data fit, k_{on} and k_{off} rate constants were obtained, and a K_D of 0.23 nM was calculated. This latter value is close to the one determined by Surface

Plasmon Resonance (SPR) measurement in a previous work although the surface chemistry used for DCF immobilization was different in this experiment (0.15 nM).[15]

With a flowrate of 25 µL/min, the frequency shift measured after 120 min of antibody injection at 1 mg/L was of -74 Hz (Figure S7). The following QCM-D experiments were conducted at this flowrate, also allowing to reduce mAb consumption.

Combined QCM-D & LSPR measurements. Binding of mAb to the sensing layer was also investigated on nanostructured sensors, allowing combined piezoelectric and optical transduction of the binding event by QCM-D and LSPR, respectively. This simultaneous real-time measurement, under the same experimental conditions and on the same surface, provides complementary information as both changes in acoustic (m_{QCM-D}) and optical mass (m_{LSPR}) uptakes. The nanostructured sensors consist in silica-coated QCM-D sensors comprising, beneath the silica layer, randomly distributed gold nanodisks, thus allowing to use the same surface chemistry than above.

The resulting combined measurement data for QCM-D (frequency and dissipation shifts) and LSPR (LSPR peak position shift) are shown in Figure 4. Before mAb injection, stabilization was performed by flowing running buffer at 25 µL/min. Injection of mAb (5 mg/L) led to a decrease in the frequency and a slight increase in dissipation energy values, respectively -62 Hz and 0.9 x 10^{-6} after 120 min (Figure 4A). Simultaneous LSPR measurement led to a $\Delta\lambda_{max}$ red-shift of around 1.40 nm upon antibody recognition (Figure 4C).

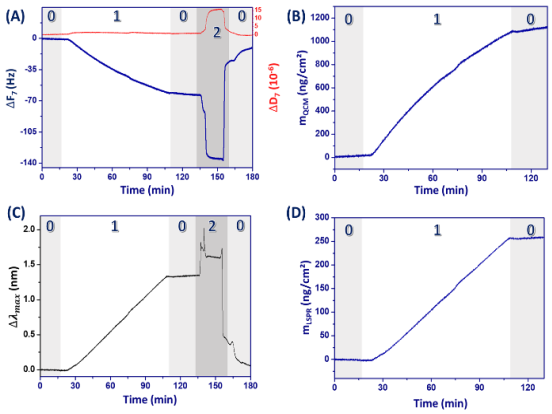

Figure 4. Adsorption of mAb (5 mg/L) by DCF-modified nanostructured quartz sensor at 25 µL/min: (A) QCM-D frequency and dissipation shifts and (B) the corresponding acoustic mass obtained from the Sauerbrey equation. (C) LSPR peak shift $\boldsymbol{\Delta\lambda}_{max}$ simultaneously recorded on the same substrate and (D) the corresponding optical mass calculated from LSPR measurement. (0) running buffer, (1) mAb adsorption, (2) regeneration.

The acoustic mass uptake (mAb and coupled solvent) was estimated from QCM-D data by applying the Sauerbrey equation, which reached ca. 1120 ng/cm² after 120 min (Figure 4B). On the other hand, the optical mass uptake was calculated from LSPR signal shift, and plateaued around 260 ng/cm² as shown in Figure 4D (detailed calculation is presented in Supporting Information). The optical mass uptake is considered as more representative of the real surface coverage as it only takes into account the antibody mass without interference from solvent molecules trapped with the protein layer. This experimental surface coverage value is consistent with the formation of a monolayer of antibodies with a head-on orientation.[33,34] Performing the measurement on the same surface and in identical experimental conditions allows an accurate comparison of both acoustic and optical mass uptakes. Hence, the percentage of coupled water to the antibody layer was calculated using equation (3), giving a hydration value of ~ 77% from data presented in Figure 5. This result is

consistent with values found in the literature for proteins adsorption onto planar surfaces[35,36] or colloidal systems.[37]

$$(3)\quad \%coupled\ water = \left(\frac{m_{QCM-D} - m_{LSPR}}{m_{QCM-D}}\right) * 100$$

Unlike the previous systems, nanostructured sensors regeneration could not be achieved (the frequency did not return to its initial value and stabilized around -10 Hz while LSPR signal returned to its baseline level), see Figure 4. Several attempts were conducted by flowing successively the regeneration and running buffers onto a DCF-functionalized nanostructured substrate (Figure S8). No return to the baseline level was observed after the first, second and third cycles of regeneration which might be attributed to a reorganization of the PEG layer on the nanostructured surface. Consequently, at this stage combined QCM-D and LSPR measurements could not be used for DCF biosensing and we focus in what follows on QCM-D.

DCF Biosensing in buffers. The principle of detection of DCF relies on a competitive assay for which binding of high affinity mAb to the DCF-containing sensing layer is inhibited by DCF in solution. To this purpose, standard solutions of DCF (0 – 333.2 nM) in running buffer were mixed with mAb (5 mg/L), incubated during one hour and then flowed over the DCF functionalized sensor for 60 min followed by a 15 min washing step with running buffer (Figure 5A). Upon injection of the mixtures of DCF and mAb, the free antibodies interacted with the immobilized DCF and generated a frequency decrease inversely related to the concentration of DCF in solution (Figure 5A). Indeed, when the concentration was small, there was no significant impact on the frequency shift. Conversely, injection of mixture of anti-DCF and a high concentration of DCF (333.2 nM) did not result in any change of frequency, indicating complete inhibition of antibody binding to the surface and absence of non-specific response.

A calibration curve for which the frequency shift measured between 0 and 60 min is plotted as a function of the DCF concentration in logarithmic scale is shown in Figure 5B. Non-linear regression of data was performed with a four-parameter logistic curve according to equation (4), where F is the signal response at DCF concentration [DCF], and B (bottom) and T (top) are the asymptotic ends corresponding to the signal at nil and infinite DCF concentrations.

$$(4)\quad F = B + \frac{(T - B)}{1 + (\frac{IC_{50}}{[DCF]})^{HS}}$$

The inflection point of the sigmoid curve (IC_{50}) defined as the DCF concentration yielding a 50% signal decrease was 40 ± 2.4 nM (12 ± 0.7 µg/L). Other fitting parameters are summed in Table S4. The limit of detection (LoD), the limit of quantitation (LoQ) and dynamic range (DR) of the assay were calculated from the calibration curve presented in Figure S9. This calibration curve was produced by normalizing the QCM-D data to blank sample response (ΔF_0). The LoD and LoQ values respectively represent the IC_{90} and IC_{80}, which are the DCF concentrations for which the QCM-D signal is 90 and 80 % of the one obtained for the blank sample in a competitive assay. The dynamic range (DR) is defined as the DCF concentration values for which the sensor signal is 20 and 80 % (IC_{80} and IC_{20}) of $\Delta F/\Delta F(0)$.

This experiment was also conducted with standard solutions of DCF in PBS (0 – 330 nM) with each sample analyzed in triplicate (*i.e.* three different sensor chips). QCM-D data and the resulting calibration curve from average △F values are respectively presented in Figure 5C and Figure 5D. The individual calibration curves and fitting parameters are presented in Figure S10A and Table S4, respectively. An IC_{50} of 28.22 ± 0.49 nM (8.36 ± 0.15 µg/L) was determined by fitting the data with the four-parameter logistic curve (equation 4).

The determined analytical parameters for both assays performed in PBS/EtOH and PBS are summarized in Table 1. The LoD was lower in PBS/EtOH while in PBS we obtained a lower LoQ and a DR centered on lower DCF concentrations. Therefore, in what follows PBS will be preferred as buffer for water resources analysis.

Table 1. Limit of detection (LoD), limit of quantification (LoQ) and dynamic range (DR) for the competitive assay of DCF in PBS/EtOH and PBS.

	PBS/EtOH	PBS
LoD (nM)	6.9	9.5
LoD (µg/L)	2.0	2.8
LoQ (nM)	24.4	15.3
LoQ (µg/L)	7.2	4.5
DR (nM)	24.4 – 56.1	15.3 – 46.1
DR (µg/L)	7.2 – 16.6	4.5 – 13.6

The LoD obtained here are in the same range, even slightly lower, that those obtained by advanced chromatographic methods, HPLC-MS (3 µg/L).[6] In addition, the analytical performances of the piezoelectric immunosensor compare favorably with previously reported label-free immunoassays. Steinke et al. developed an optical immunoassay, using the same mAb, which presented a detection range in the µg/L window.[18] Rau et al. proposed another optical immunoassay for DCF with a LoD of 0.2842 µg/L and a LoQ of 0.4933 µg/L in buffer.[27] This better sensitivity might be due to the use of aceclofenac instead of DCF as a less competitive immobilized ligand. More detailed information on the analytical performances of biosensors already reported for diclofenac quantification in various media are gathered in Table S7.

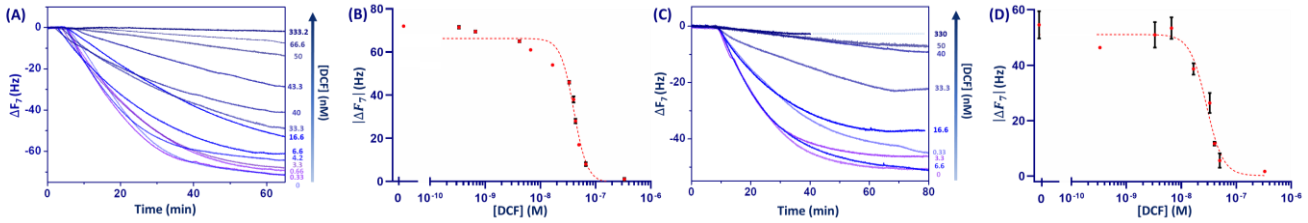

Figure 5. Competitive immunoassay established from frequency shifts measured during injection of mixtures of mAb (5 mg/L) and DCF (0 -333.2 nM) at flow rate of 25 µL/min (A) in PBS/EtOH with (B) corresponding calibration curve; (C) in PBS with (D) corresponding calibration curve. QCM-D values are summarized in Table S6 and fitting parameters are detailed in Table S4.

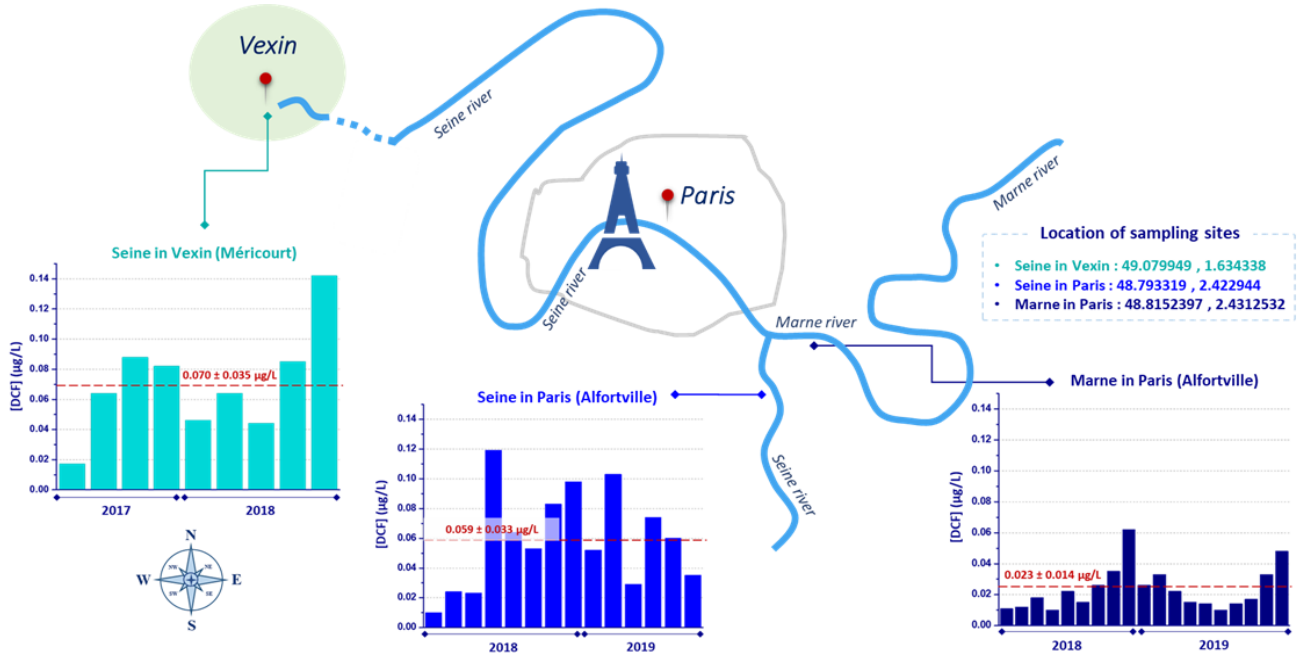

Figure 6. Sampling sites of surface water collected in the Marne river in Paris and the Seine river in Paris and Vexin; and corresponding DCF concentrations determined by eaufrance agency[38] with average values.

DCF quantification in surface water samples. The competitive immunoassay was applied to the quantification of DCF in surface water samples collected in the Seine river at two locations (Paris and Vexin, France) and the Marne river in Paris as presented in Figure 6.

Prior to the analysis, the collected samples were concentrated 100-fold by solid phase extraction (SPE) following a procedure described in the experimental section. All samples were analyzed in triplicate (*i.e.* three different sensor chips) and the corresponding sensorgrams are presented in Figure 7 and summarized in Table 2 with average values. Upon analysis of surface water samples and using the individual calibration curves established from DCF standards in PBS (Figure S10), DCF concentrations of 23.2 ± 1.5 nM (6.9 ± 0.5 µg/L) and 14.4 ± 0.2 nM (4.27 ± 0.06 µg/L) were calculated for the Seine river in Vexin and Paris, respectively. DCF concentration in Marne water was found below the calculated LoD of the analytical system.

Considering the pre-concentration by 100-fold and assuming no loss during SPE procedure, the DCF concentration in the Seine water would be of 0.0687 ± 0.0049 µg/L and 0.0427 ± 0.0006 µg/L for the Seine river in Vexin and Paris, respectively. These values are consistent with data provided by eaufrance agency[38] (Figure 6) and are also lower than the guide value given by ANSES (0.4 µg/L).[5] Attempts to assay the same pre-concentrated river samples by RP-HPLC were unsuccessful (see Figure S11).

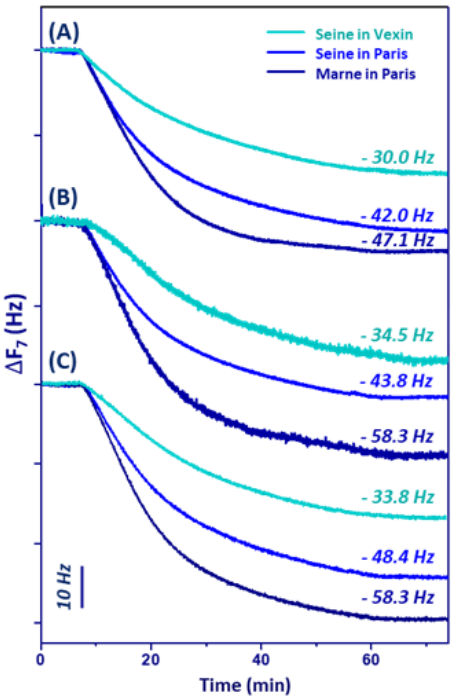

Figure 7. QCM-D frequency shifts for the competitive immunoassay of DCF in surface water samples performed by flowing mAb (5 mg/L) in PBS buffer at 25 µL/min for (A) sensor 1, (B) sensor 2 and (C) sensor 3. QCM-D data are summarized in Table S8.

Table 2. DCF concentration in three different surface water samples as calculated from the calibration curve established in PBS and shown in Figure S10.

	Seine in Vexin		**Seine in Paris**		**Marne in Paris**	
	[DCF] (nM)	[DCF] (µg/L)	[DCF] (nM)	[DCF] (µg/L)	[DCF] (nM)	[DCF] (µg/L)
Sensor 1	23.8	7.1	14.2	4.2	< LoD	< LoD
Sensor 2	21.4	6.3	14.5	4.3	< LoD	< LoD
Sensor 3	24.3	7.2	14.6	4.3	< LoD	< LoD
Average values	23.2 ± 1.5	6.9 ± 0.5	14.4 ± 0.2	4.27 ± 0.06		

CONCLUSIONS

In this work, we designed a competitive piezoelectric immunosensor to assay diclofenac in water resources. A sensing layer comprising diclofenac as competitor was built up layer-by-layer by a wet chemistry process on silica-coated quartz sensor chips. Diclofenac immobilization to the amine-terminated PEG layer was investigated using three different activation strategies and the PyBOP chemistry was selected for further experiments. Binding of a highly affine monoclonal antibody to immobilized diclofenac was investigated by combining, in real time, QCM-D and LSPR. These measurements allowed to calculate a dissociation constant K_D of 0.24 nM and an optical mass uptake of 260 ng/cm² upon antibody binding, in excellent agreement with the formation of a monolayer of antibodies in a head-on orientation. A hydration percentage of ca. 75% was determined for the antibody layer. A competitive QCM-D assay was then set up for the detection of diclofenac for which

binding of antibody to the DCF-containing sensing layer is inhibited by DCF in solution. The sensor response expressed as frequency shift $\triangle F$ was inversely related to the concentration of DCF in solution with a dynamic range of 15 – 46 nM and a limit of detection of 9.5 nM (2.8 µg/L) in PBS. Finally, this piezoelectric immunosensor was applied to the analysis of surface water samples taken at three locations in the rivers Seine and Marne. The calculated concentration of DCF in these samples was in good agreement with data published by eaufrance agency which collection requires extremely heavy protocols. These finding pave the way for a rapid and easy to implement assay of small pollutants in river water.

ASSOCIATED CONTENT

SUPPORTING INFORMATION

Materials, surface functionalization protocols, characterization techniques presentation, baseline corrected ATR-IR spectra, table with ATR-IR assignments, WCA results, activation mechanisms of DCF, table with XPS atomic composition, XPS spectra used for DCF surface coverage determination, detailed procedure for XPS quantitative analysis, XPS analysis for sonication procedure, table with fitting parameters for K_D determination, QCM-D sensorgrams investigating effect of the flow rate on mAb adsorption, procedure for m_{LSPR} calculation, QCM-D and LSPR sensorgrams investigating effect of regeneration on the PEG layer on nanostructured sensor, calibration curve in PBS/EtOH, calibration curves in PBS, table with fitting parameters of the logistic fit in PBS/EtOH and PBS, table presenting the determined LoD, LoQ and DR in PBS/EtOH and PBS, table presenting QCM-D data for the competitive immunoassay in PBS/EtOH and PBS, QCM-D data for the competitive immunoassay in surface water rivers.

The Supporting information is available free of charge via the Internet at http://pubs.acs.org.

AUTHOR INFORMATION

Corresponding Author

Souhir Boujday - Sorbonne Université, CNRS, Laboratoire de Réactivité de Surface (LRS), 4 place Jussieu, F-75005 Paris, France

Email: souhir.boujday@sorbonne-universite.fr

Michèle Salmain - Sorbonne Université, CNRS, Institut Parisien de Chimie Moléculaire (IPCM), 4 place Jussieu F-75005 Paris, France

Email: michele.salmain@sorbonne-universite.fr

Author Contributions

The manuscript was written through contributions of all authors. All authors have given approval to the final version of the manuscript.

Funding Sources

None

Notes

None

ACKNOWLEDGMENT

This work was supported by the French-Austrian ANR-FWF programme, project NanoBioSensor [grant ANR-15-CE9-0026-02].

ABBREVIATIONS

DCF, Diclofenac; NSAID, Non-steroidal anti-inflammatory drug; QCM-D, Quartz Crystal Microbalance with Dissipation measurement; SPE, Solid Phase Extraction; XPS, X-ray Photoelectron Spectroscopy; ATR-IR, Attenuated total reflection-Infrared; WCA, water contact angle; k_{on}, association constant rate; k_{off}, dissociation constant rate; K_D, dissociation constant; m_{QCM-D}, acoustic mass; m_{LSPR}, optical mass: LoD, Limit of Detection; LoQ, Limit of Quantification; DR, Dynamic Range; mAb, monoclonal Antibody;

REFERENCES

(1) Bregoli, F.; Acuña, V.; Barceló, D.; Corominas, L.; Ginebreda, A.; Petrovic, M.; Rodríguez-Roda, I.; Sabater, S.; Marcé, R. The fate of pharmaceuticals in freshwaters: a new global model for decision making | IHE Delft Institute for Water Education https://www.un-ihe.org/news/fate-pharmaceuticals-freshwaters-new-global-model-decision-making (accessed 2020 -12 -21).

(2) Vella, K. *Commission Implementing Decision (EU) 2015/495 of 20 March 2015 Establishing a Watch List of*

Substances for Union-Wide Monitoring in the Field of Water Policy Pursuant to Directive 2008/105/EC of the European Parliament and of the Council (Notified under Document C(2015) 1756) Text with EEA Relevance; 2015; Vol. 078.

(3) Sousa, J. C. G.; Ribeiro, A. R.; Barbosa, M. O.; Pereira, M. F. R.; Silva, A. M. T. A Review on Environmental Monitoring of Water Organic Pollutants Identified by EU Guidelines. *J. Hazard. Mater.* **2018**, *344*, 146–162.

(4) Lonappan, L.; Brar, S. K.; Das, R. K.; Verma, M.; Surampalli, R. Y. Diclofenac and Its Transformation Products: Environmental Occurrence and Toxicity - A Review. *Environ. Int.* **2016**, *96*, 127–138.

(5) ANSES. Site | Anses - Agence nationale de sécurité sanitaire de l'alimentation, de l'environnement et du travail https://www.anses.fr/fr/search/site/EAUX2016SA0135?iso1=fr&iso2=en (accessed 2020 -12 -21).

(6) Schmidt, S.; Hoffmann, H.; Garbe, L.-A.; Schneider, R. J. Liquid Chromatography–Tandem Mass Spectrometry Detection of Diclofenac and Related Compounds in Water Samples. *J. Chromatogr. A* **2018**, *1538*, 112–116.

(7) Kafeenah, H. I. S.; Osman, R.; Bakar, N. K. A. Disk Solid-Phase Extraction of Multi-Class Pharmaceutical Residues in Tap Water and Hospital Wastewater, Prior to Ultra-Performance Liquid Chromatographic-Tandem Mass Spectrometry (UPLC-MS/MS) Analyses. *RSC Adv.* **2018**, *8* (70), 40358–40368.

(8) Raysyan, A.; Moerer, R.; Coesfeld, B.; Eremin, S. A.; Schneider, R. J. Fluorescence Polarization Immunoassay for the Determination of Diclofenac in Wastewater. *Anal. Bioanal. Chem.* **2021**, *413* (4), 999–1007.

(9) Yang, X.; Wang, Y.; Yang, J.; Sun, Z.; Chu, C.; Yue, Z.; Li, L.; Hu, X. Development of an Immunochromatographic Lateral Flow Strip Test for the Rapid Detection of Diclofenac in Medicinal Wine. *Food Agric. Immunol.* **2020**, *31* (1), 205–216.

(10) Carl, P.; Sarma, D.; Gregório, B. J. R.; Hoffmann, K.; Lehmann, A.; Rurack, K.; Schneider, R. J. Wash-Free Multiplexed Mix-and-Read Suspension Array Fluorescence Immunoassay for Anthropogenic Markers in Wastewater. *Anal. Chem.* **2019**, *91* (20), 12988–12996.

(11) Deng, D.; Yang, H.; Liu, C.; Zhao, K.; Li, J.; Deng, A. Ultrasensitive Detection of Diclofenac in Water Samples by a Novel Surface-Enhanced Raman Scattering (SERS)-Based Immunochromatographic Assay Using AgMBA@SiO2-Ab as Immunoprobe. *Sensor Actuat. B-Chem.* **2019**, *283*, 563–570.

(12) Wang, C.; Jiang, T.; Zhao, K.; Deng, A.; Li, J. A Novel Electrochemiluminescent Immunoassay for Diclofenac Using Conductive Polymer Functionalized Graphene Oxide as Labels and Gold Nanorods as Signal Enhancers. *Talanta* **2019**, *193*, 184–191.

(13) Hlaváček, A.; Peterek, M.; Farka, Z.; Mickert, M. J.; Prechtl, L.; Knopp, D.; Gorris, H. H. Rapid Single-Step Upconversion-Linked Immunosorbent Assay for Diclofenac. *Microchim. Acta* **2017**, *184* (10), 4159–4165.

(14) Hlaváček, A.; Farka, Z.; Hübner, M.; Horňáková, V.; Němeček, D.; Niessner, R.; Skládal, P.; Knopp, D.; Gorris, H. H. Competitive Upconversion-Linked Immunosorbent Assay for the Sensitive Detection of Diclofenac. *Anal. Chem.* **2016**, *88* (11), 6011–6017.

(15) Huebner, M.; Weber, E.; Niessner, R.; Boujday, S.; Knopp, D. Rapid Analysis of Diclofenac in Freshwater and Wastewater by a Monoclonal Antibody-Based Highly Sensitive ELISA. *Anal. Bioanal. Chem.* **2015**, *407* (29), 8873–8882.

(16) Kaewwonglom, N.; Oliver, M.; Cocovi-Solberg, D. J.; Zirngibl, K.; Knopp, D.; Jakmunee, J.; Miro, M. Reliable Sensing Platform for Plasmonic Enzyme-Linked Immunosorbent Assays Based on Automatic Flow-Based Methodology. *Anal. Chem.* **2019**, *91* (20), 13260–13267.

(17) Shi, J.; Xu, M.; Tang, Q.; Zhao, K.; Deng, A.; Li, J. Highly Sensitive Determination of Diclofenac Based on Resin Beads and a Novel Polyclonal Antibody by Using Flow Injection Chemiluminescence Competitive Immunoassay. *Spectrochim. Acta. A. Mol. Biomol. Spectrosc.* **2018**, *191*, 1–7.

(18) Steinke, N.; Döring, S.; Wuchrer, R.; Kroh, C.; Gerlach, G.; Härtling, T. Plasmonic Sensor for On-Site Detection of Diclofenac Molecules. *Sensor Actuat. B-Chem.* **2019**, *288*, 594–600.

(19) Kassahun, G. S.; Griveau, S.; Juillard, S.; Champavert, J.; Ringuedé, A.; Bresson, B.; Tran, Y.; Bedioui, F.; Slim, C. Hydrogel Matrix-Grafted Impedimetric Aptasensors for the Detection of Diclofenac. *Langmuir* **2020**, *36* (4), 827–836.

(20) Shi, T.; Wen, Z.; Ding, L.; Liu, Q.; Guo, Y.; Ding, C.; Wang, K. Visible/near-Infrared Light Response VOPc/Carbon Nitride Nanocomposites: VOPc Sensitizing Carbon Nitride to Improve Photo-to-Current Conversion Efficiency for Fabricating Photoelectrochemical Diclofenac Aptasensor. *Sensor Actuat. B-Chem.* **2019**, *299*, 126834.

(21) Schirmer, C.; Posseckardt, J.; Kick, A.; Rebatschek, K.; Fichtner, W.; Ostermann, K.; Schuller, A.; Rödel, G.; Mertig, M. Encapsulating Genetically Modified Saccharomyces Cerevisiae Cells in a Flow-through Device towards the Detection of Diclofenac in Wastewater. *J. Biotechnol.* **2018**, *284*, 75–83.

(22) Schirmer, C.; Posseckardt, J.; Schröder, M.; Gläser, M.; Howitz, S.; Scharff, W.; Mertig, M. Portable and Low-Cost Biosensor towards on-Site Detection of Diclofenac in Wastewater. *Talanta* **2019**, *203*, 242–247.

(23) Guenther, M.; Altenkirch, F.; Ostermann, K.; Rödel, G.; Tobehn-Steinhäuser, I.; Herbst, S.; Görlandt, S.; Gerlach, G. Optical and Impedimetric Study of Genetically Modified Cells for Diclofenac Sensing. *J. Sens. Sens. Syst.* **2019**, *8* (1), 215–222.

(24) Nguyen, T. T. K.; Vu, T. T.; Anquetin, G.; Tran, H. V.; Reisberg, S.; Noël, V.; Mattana, G.; Nguyen, Q. V.; Dai Lam, T.; Pham, M. C.; Piro, B. Enzyme-Less Electrochemical Displacement Heterogeneous Immunosensor for Diclofenac Detection. *Biosens. Bioelectron.* **2017**, *97*, 246–252.

(25) Azadbakht, A.; Beirnvand, S. Voltammetric Aptamer-Based Switch Probes for Sensing Diclofenac Using a Glassy Carbon Electrode Modified with a Composite Prepared from Gold Nanoparticles, Carbon Nanotubes and Amino-Functionalized Fe3O4 Nanoparticles. *Microchim. Acta* **2017**, *184* (8), 2825–2835.

(26) Kashefi-Kheyrabadi, L.; Mehrgardi, M. A. Design and Construction of a Label Free Aptasensor for Electrochemical Detection of Sodium Diclofenac. *Biosens. Bioelectron.* **2012**, *33* (1), 184–189.

(27) Rau, S.; Hilbig, U.; Gauglitz, G. Label-Free Optical Biosensor for Detection and Quantification of the Non-

Steroidal Anti-Inflammatory Drug Diclofenac in Milk without Any Sample Pretreatment. *Anal. Bioanal. Chem.* **2014**, *406* (14), 3377–3386.
(28) Steinke, N.; Rio, M.; Wuchrer, R.; Schuster, C.; Ljasenko, E.; Knopp, D.; Gerlach, G.; Härtling, T. Detection of Diclofenac Molecules by Planar and Nanostructured Plasmonic Sensor Substrates. *Sensor Actuat. B-Chem.* **2018**, *254*, 749–754.
(29) Huebner, M.; Ben Haddada, M.; Méthivier, C.; Niessner, R.; Knopp, D.; Boujday, S. Layer-by-Layer Generation of PEG-Based Regenerable Immunosensing Surfaces for Small-Sized Analytes. *Biosens. Bioelectron.* **2015**, *67*, 334–341.
(30) Ben Haddada, M.; Huebner, M.; Casale, S.; Knopp, D.; Niessner, R.; Salmain, M.; Boujday, S. Gold Nanoparticles Assembly on Silicon and Gold Surfaces: Mechanism, Stability, and Efficiency in Diclofenac Biosensing. *J. Phys. Chem. C* **2016**, *120* (51), 29302–29311.
(31) Höök, F.; Rodahl, M.; Brzezinski, P.; Kasemo, B. Energy Dissipation Kinetics for Protein and Antibody−Antigen Adsorption under Shear Oscillation on a Quartz Crystal Microbalance. *Langmuir* **1998**, *14* (4), 729–734.
(32) Oshannessy, D. J.; Brighamburke, M.; Soneson, K. K.; Hensley, P.; Brooks, I. Determination of Rate and Equilibrium Binding Constants for Macromolecular Interactions Using Surface Plasmon Resonance: Use of Nonlinear Least Squares Analysis Methods. *Anal. Biochem.* **1993**, *212* (2), 457–468.
(33) Boujday, S.; Bantegnie, A.; Briand, E.; Marnet, P.-G.; Salmain, M.; Pradier, C.-M. In-Depth Investigation of Protein Adsorption on Gold Surfaces: Correlating the Structure and Density to the Efficiency of the Sensing Layer. *J. Phys. Chem. B* **2008**, *112* (21), 6708–6715.
(34) Zhang, L.; Mazouzi, Y.; Salmain, M.; Liedberg, B.; Boujday, S. Antibody-Gold Nanoparticle Bioconjugates for Biosensors: Synthesis, Characterization and Selected Applications. *Biosens. Bioelectron.* **2020**, *165*, 112370.
(35) Vörös, J. The Density and Refractive Index of Adsorbing Protein Layers. *Biophys. J.* **2004**, *87* (1), 553–561.
(36) Ray, S.; Shard, A. G. Quantitative Analysis of Adsorbed Proteins by X-Ray Photoelectron Spectroscopy. *Anal. Chem.* **2011**, *83* (22), 8659–8666.
(37) Bell, N. C.; Minelli, C.; Shard, A. G. Quantitation of IgG Protein Adsorption to Gold Nanoparticles Using Particle Size Measurement. *Anal. Methods* **2013**, *5* (18), 4591.
(38) Naïades. Recherche | Naïades http://www.naiades.eaufrance.fr/acces-donnees#/physicochimie/resultats?debut=16-11-2017&fin=16-11-2020&parametres=5349 (accessed 2020 -12 -21).

For Table of Contents Only